Int. J. Electrochem. Sci., 7 **(2012)** 12159 - 12180

International Journal of
ELECTROCHEMICAL
SCIENCE
www.electrochemsci.org

Numerical Study on Ionic Transport through Micro-Nanochannel Systems

Reiyu Chein[*], *Bogan Chung*

Department of Mechanical Engineering, National Chung Hsing University, Taichung City, Taiwan 402
[*]E-mail: rychein@dragon.nchu.edu.tw

Received: 6 October 2012 / *Accepted:* 29 October 2012 / *Published:* 1 December 2012

We numerically study the sidewall charge effect on the ionic transport characteristics in micro-nanochannel systems. The sidewalls located at the micro-nanochannel junctions may be uncharged or charged with the same or opposite polarity as that of the nanochannel surface charge. The numerical results indicate that the concentration polarization induced potential drop at the nanochannel entrance controls the ionic current flow in the micro-nanochannel systems. When the sidewall has the same charge polarity as that of the nanochannel, a plateau (on a log-log scale) can be observed for the nanochannel conductance variation with respect to the electrolyte bulk concentration because of the enriched counterions at the nanochannel entrance. For the sidewall uncharged or charged with opposite polarity to that of the nanochannel, the conductance plateau cannot be observed in the low bulk concentration regime due to depleted counterion at the nanochannel entrance. Our result also indicates that it is possible to construct a nanofluidic switch by controlling the polarity of the sidewall surface charge when electrolyte has low bulk concentration.

Keywords: Micro-nanochannel system, sidewall charge polarity, concentration polarization, conductance plateau, and nanofluidic switch.

1. INTRODUCTION

Due to the advances in nano fabrication techniques, flow channels with nanoscale dimensions can be fabricated successfully [1]. With the channel dimension at such length scale, high surface-to-volume ratio leads to new physical phenomena that are not observed in channels with macro- or micro-scale [2]. For example, when the dimensions of the nanofluidic channel with charged surface are comparable to the Debye length, electrokinetic phenomena such as electroosmosis and streaming potential are different from those observed at microscale dimensions. Several interesting ionic transport properties in nanochannels have been revealed including ion permselectivity [3], ion enrichment and depletion [4, 5], ion current rectification [6], and channel conductance enhancement

[7]. These characteristics provides the possibility of controlling and manipulating fluids in nanochannels with potential applications in various fields such as analyte preconcentration [8, 9], molecule sensing and separation [10-12], nanofluidic diodes and transistors [13-16] and energy harvesting devices [17, 18]. It can be expected that more new physical phenomena and applications will be explored.

Among the nanofluidic researches, identifying the nanochannel electric conductance has received much attention in recent years. Stein et al. [19] carried out an experiment to measure the nanochannel conductance using KCl as the working electrolyte. They found that the channel conductance exhibits a striking saturation at a value that was independent of the channel size and bulk concentration when the bulk concentration is low. When the bulk concentration is high, the measured channel conductance varies linearly with both the channel size and bulk concentration. They attributed the low-salt ionic transport behavior in nanochannels to the electrostatic effect of the channel surface charge on the fluid. Using both nanochannel slits and cylindrical nanopores, the experimental measurements of Karnik et al. [20] also found that the electrical conductance of nanofluidic channels saturate at a value for the dilute electrolyte, which departs significantly from the bulk behavior. Schoch and Renaud [21] further experimentally showed that the nanochannel conductance depends on the pH value of the bulk electrolyte and the saturated value of nanochannel conductance can be found in the low-salt concentration regime. Liu et al. [22] discovered that the apparent proton conductivity inside a nanochannel can be enhanced by orders of magnitude relative to that in a bulk solution. Such enhancement can be found even when the electric double layers do not overlap. Along with the experimental measurements [21, 22], these studies also developed simple models to describe the nanochannel conductance and compared with the measured data.

Besides the experimental measurements, several numerical models on nanochannel conductance have been reported. Daiguji et al. [23] developed a numerical model to describe the ionic distribution in a nanochannel. They pointed out that as the nanochannel diameter is smaller than the Debye length, a unipolar solution of counterions is created inside the nanotube and the coions are electrostatically expelled. This ion enrichment and ion depletion phenomena are similar to the ion selective membrane which contains electrically charged nanopores. However, the relation between the nanochannel conductance and electrolyte bulk concentration and the effect of reservoirs were not addressed. In order to obtain the experimentally observed saturated conductance in low-salt concentration regime, there are two approaches reported in the literature. Wang et al. [24] proposed an enrichment coefficient to describe the enriched counterions inside the nanochannel in their theoretical model and the obtained electric and streaming conductances were in good agreement with the experimental data reported by Stein et al. [19] and van der Heyden et al. [25]. Choi and Kim [26] and Huang and Yang [27] added the surface conductance [28, 29] in their models to fulfill the experimental observation. However, a constant surface conductance was assumed in their models without a detailed Stern layer model. Moreover, Vlassiouk et al. [30] pointed out that in addition to the surface charge density and electrolyte bulk concentration, channel size (diameter and length) also plays an important role in the ionic current through the nanochannel.

Based on the unipolar ionic distribution in nanochannels, Daiguji et al. [13, 14] and Vlassiouk et al. [15, 16] further extended to study the characteristics of nanofluidic diodes and transistors in

which the current flow through the nanochannel can be controlled by having the surface charge with opposite polarity distributions along the channel wall. As pointed out by these studies, having the electric double layers overlap is not a required condition for controlling the current.

From practical point of view, the nanochannel must be connected with either reservoirs or large-size channels in order to carry out their applications. However, most of the studies on the ionic transport phenomena in nanofluidic devices reported in the literature focused on the nanochannel surface charge effect and the reservoir or large-size channel effect was overlooked. The study by Cheng and Guo [31] revealed the role of the surface charge density and polarity on channel entrance side-walls in affecting the ion conductance of nanochannels (or nanoslits). Reduced ion conductance was observed in the nanochannel having opposite surface charge polarity on the entrance side-walls to that in the channel and was ascribed to its function as a parasitic nanofluidic diode. In this study, the effects of surface charge density magnitude and polarity of cylindrical microchannel or reservoir wall on the ionic current through the cylindrical nanochannel is to be addressed by solving the complete Poisson-Nernst-Planck equation. Based on the current-voltage curve (I-V curve), the effect of the microchannel or reservoir wall charge on the nanochannel conductance can be obtained and compared with the experimental observations.

2. PHYSICAL MODEL

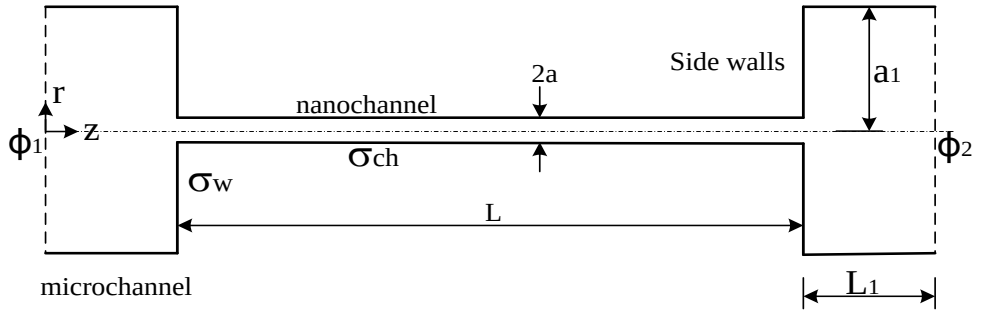

Figure 1. Schematic diagram of the micro-nanochannel system. The nanochannel wall and sidewall surface charge densities are σ_{ch} and σ_w, respectively.

We consider a circular nanochannel having a length of L and radius of a, as shown in Figure 1. The nanochannel wall can be either negatively or positively charged with a surface charge density of σ_{ch}. At the ends of the nanochannel, two microchannels with length of L_1 and radius of a_1 are connected. The ends of the microchannel can be regarded as the interfaces between the microchannels and well-stirred electrode compartments at which the potential bias $\Delta\phi = \phi_1 - \phi_2$ is applied. The resulting electric field is in the positive z direction when $\Delta\phi > 0$ and in the negative z direction as $\Delta\phi < 0$.We assume that an aqueous salt solution with a bulk molar concentration c_0 entirely fills the

system and the system is in equilibrium when $\Delta\phi = 0$. The physical domain considered in this study is similar to the study of Postler et al. [32] and can also be regarded as a theoretical model for studying the ionic flow behavior in the ion exchange membranes [33].

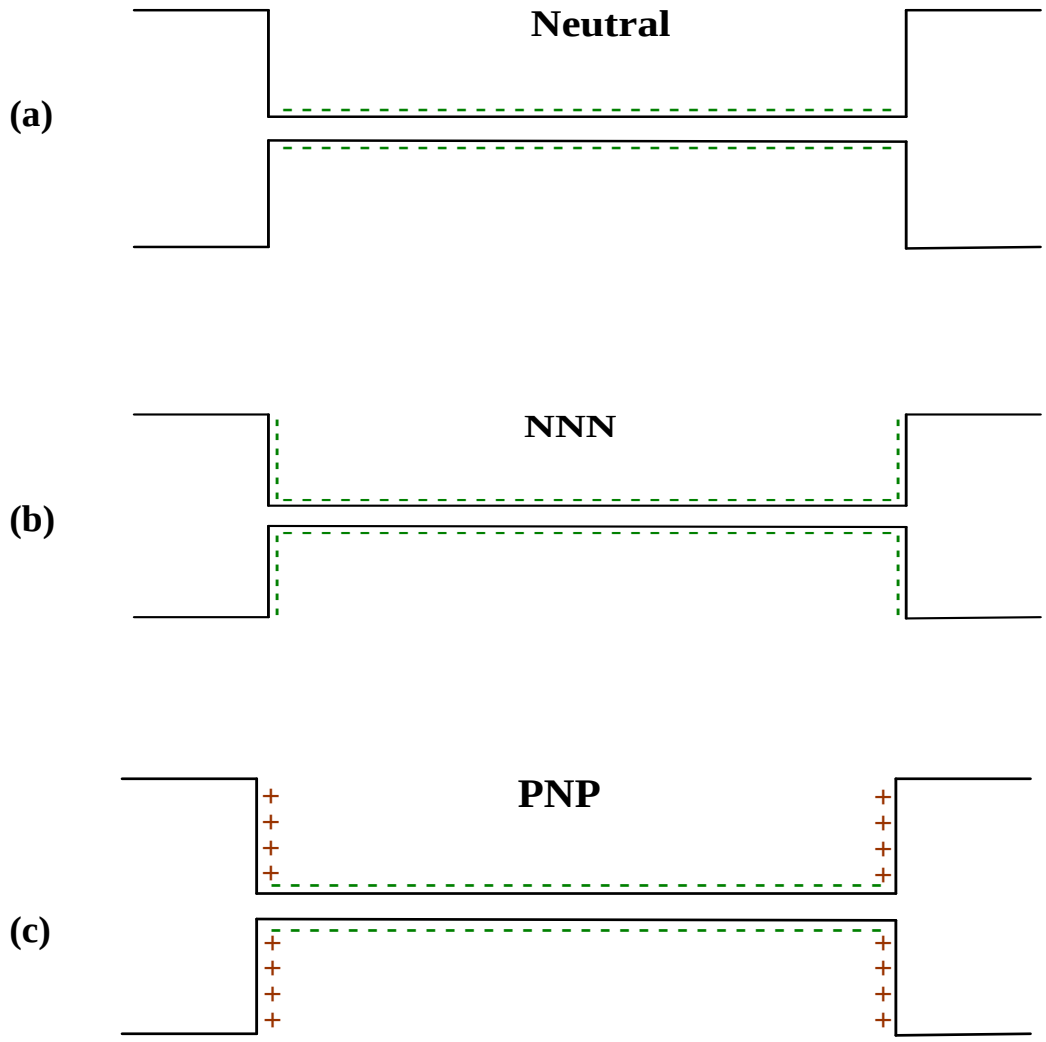

Figure 2. Surface charge density arrangements investigated in this study. The positive and negative signs indicate the wall is either positively or negatively charged. (a) Neutral channel. (b) NNN channel. (c) PNP channel.

Based on the physical model shown in Figure 1, there are two sidewalls having the same radius as that of the microchannel. From the fabrication point of view, the channels may be made of the same substrate and therefore all of the channel walls possess the same electrochemical properties as they are in contact with the electrolyte. As mentioned in the study by Vlassiouk et al. and Siwy et al. [16, 34], the surface charge density can be altered either passively by controlling the pH value of the bulk electrolyte or actively using coating layers with a different chemical composition from the substrate. Cheng and Gao [35] successfully demonstrated that an Al_2O_3 layer can be coated onto fuse silica-made

micro-nanochannel devices, resulting in different charge polarities along the channel wall. In this study, we consider that the sidewalls at the microchannel/nanochannel junctions can be either positively or negatively charged with surface charge density of σ_w while the rest of the microchannel walls remain uncharged for simplifying the analysis.

When the surface charge densities of the nanochannel and sidewall have different polarity, it acts like a nanofluidic diode at the entrance and exit of the nanochannel. These diodes are different from those studied by Daiguji et al. and Vlassiouk et al. [13-16] in which the charge polarity difference was made along the nanochannel wall. Figure 2 shows the surface charge density arrangements considered in this study. For convenience in discussion, the channel is denoted as Neutral channel when the sidewall is uncharged, NNN channel when both the sidewall and nanochannel are negatively charged, and PNP channel when the sidewalls have opposite polarity to that of the nanochannel wall. The surface charge arrangement in PNP channels can be regarded as two nanofluidic diodes located at the ends of the nanochannel, operated either in forward or backward direction depending on the applied electric field direction. Note that the surface charge polarity can also be arranged reversely for Neutral, NNN, and PNP channels shown in Figure 2. In such case, the counterion and coion switch their role. For a binary electrolyte such as KCl, the ionic transport characteristics would be approximately the same because the electric mobilities of both K^+ and Cl^- ions are approximately equal. The inclusion of charge density along the sidewalls is expected to produce counterion enrichment or depletion in the regions at the nanochannel entrance and exit. This leads to either decrease or increase the access resistance and may have a significant effect on the overall ionic transport through the nanochannel [36].

3. SIMPLE MODELS

Using aqueous KCl solution as the electrolyte, Schoch and Renaud [21] provided a simple model to describe the negative nanoslit conductance based on the effective surface charge density. For cylindrical nanochannel, this model can be rewritten as,

$$G = F^2 c_0 \frac{\pi a^2}{L}(m_{K^+} + m_{Cl^-}) + F^2 m_{K^+} c_e \frac{\pi a^2}{L} \tag{1}$$

where c_e is the excess counterion concentration which can be calculated from the requirement of overall electroneutrality,

$$c_e = \frac{2|\sigma|}{aF} \tag{2}$$

In Eq. (1), G is the nanochannel conductance, F is the Faraday number, and m_{K^+} and m_{Cl^-} are the electric mobilities of K^+ and Cl^-, respectively. The first term on the right hand side is the bulk

conductance contributed by the bulk electrolyte while the second term accounts for the surface charge effect on the conductance. Because of ion selectivity feature of the charged nanochannel, counterion is increased and coion is decreased inside the nanochannel. In order to take the concentration effect into account, Wang et al. [24] and Huang and Yang [27] introduced the effective bulk ionic concentration to correct the contribution of bulk conductance. Accordingly, Eq. (1) is modified as,

$$G = F^2 c_0 \frac{\pi a^2}{L}(\alpha m_{K^+} + \beta m_{Cl^-}) + F m_{K^+} \frac{2\pi a|\sigma|}{L} \tag{3}$$

Where α and β can be interpreted as the degrees of counterion increase and coion decrease in the nanochannel due to surface charge density and can be defined as,

$$\alpha = \frac{1}{\pi a^2 c_0}\int_0^a c_{K^+} 2\pi r dr\,,\ \beta = \frac{1}{\pi a^2 c_0}\int_0^a c_{Cl^-} 2\pi r dr \tag{4}$$

As shown by Schoch and Renaud [21], the nanoslit conductance predicted using the simple model is in good agreement with their experimental measurements. Therefore, Eq. (3) can be used as a comparison basis for the numerical model. For the uncharged channel ($\sigma_w = \sigma_{ch}$ =0), the nanochannel conductance including the Hall resistance can be described as [37],

$$G_0 = F^2 c_0 (m_{K^+} + m_{Cl^-})(4a + \frac{\pi a^2}{L}) \tag{5}$$

4. TWO-DIMENSIONAL MODEL

Numerical simulation is employed to elicit greater understanding of the surface charge density distribution effect on the ionic transport in nanochannels of various dimensions. Because the continuum hypothesis has been shown to be appropriate for nanochannels with diameters larger than 2.2 nm [38, 39], ionic flux in the nanochannel is described using the Nernst-Planck equation for each species,

$$\vec{J}_i = -D_i \nabla c_i + m_i z_i c_i \nabla(\phi + \psi) + c_i \vec{V} \tag{6}$$

where $\vec{J}_i$, D_i, m_i, c_i, z_i, and $\vec{V}$ are, respectively, the ionic flux, molecular diffusivity, electrical mobility, concentration, charge valance of ith ion, and electrolyte flow velocity. ϕ and ψ are the local electrical potential due to the externally applied potential bias and potential due to the surface charge density on the wall. The distributions of ϕ and ψ are described by the Laplace and Poisson equations, respectively,

$$\nabla^2 \phi = 0 \tag{7}$$

$$\nabla^2\psi = -\frac{\rho_e}{\varepsilon\varepsilon_0} \tag{8}$$

In Eq. (8), ε is the dielectric permittivity, ε_0 is the permittivity of vacuum, and ρ_e is the space charge density defined as,

$$\rho_e = F\sum_{i=1}^{N} z_i c_i \tag{9}$$

where N is the number of ions. For dilute electrolytes, the ion electrical mobility can be related to the molecular diffusivity D_i using the Nernst-Einstein equation as [40],

$$m_i = \frac{D_i}{RT} \tag{10}$$

where R is the universal gas constant and T is the fluid temperature. For steady state and no species generation or destruction source, the ionic flux satisfies,

$$\nabla \cdot \vec{J}_i = 0 \tag{11}$$

As potential bias is applied, the electroosmotic flow (EOF) will be induced due to the interaction between the electric double layer and potential bias. The governing equation describing the fluid flow is the modified Navier-Stokes equation written as,

$$\nabla \cdot \vec{V} = 0 \tag{12a}$$

$$\vec{V} \cdot \nabla\vec{V} = -\nabla p + \mu\nabla^2\vec{V} - \rho_e\nabla(\phi + \psi) \tag{12b}$$

where p is the pressure and μ is the viscosity. The last term on the right-hand side of Eq. 12(b) is known as the electric body force per unit volume when electro-striction and the permittivity gradient in the electrical field are ignored. After solving Eqs. (7)-(12) with appropriate boundary conditions, the current density in the flow field can be calculated as,

$$\vec{i} = -\Lambda\nabla(\phi + \psi) - F\sum z_i D_i \nabla c_i + F\vec{V}\sum z_i c_i \tag{13}$$

where $\Lambda = F^2\sum {z_i}^2 m_i c_i$ is the electrolyte electrical conductivity. By integrating Eq. (12) through any cross sectional area of the micro-nanochannel system, the total current through the nanochannel can be obtained. In Eq. (13), the terms on the right-hand side are currents due to ion electromigration, diffusion, and convection, respectively.

All governing equations were written in a cylindrical coordinate system (r, θ, z). Utilizing the symmetry in the θ coordinate, we can recast the problem as an axisymmetric two-dimensional model (r, z). The fluid velocity components in the r- and z-directions are u and v, respectively. Because of the geometrical symmetry the computational domain is taken as half the physical domain as shown in Figure 3. Based on the physical model described in Section 2, the boundary conditions required to solve Eqs. (7)-(12) are specified as follows:

Figure 3. Computational domain in numerical simulation.

Boundary AB :

$$\psi = 0, \phi = \phi_1, \; c_i = c_0, \; p = 0 \tag{14a}$$

Boundaries: BC and FG:

$$\frac{\partial \psi}{\partial r} = \frac{\partial \phi}{\partial r} = \frac{\partial c_i}{\partial r} = 0, \; u = v = 0 \tag{14b}$$

Boundaries CD and FE:

$$\frac{\partial c_i}{\partial z} = \frac{\partial \phi}{\partial z} = 0, \; \frac{\partial \psi}{\partial z} = -\frac{\sigma_w}{\varepsilon \varepsilon_0}, \; u = v = 0 \tag{14c}$$

Boundary DE:

$$\frac{\partial \phi}{\partial r} = 0, \; \frac{\partial \psi}{\partial r} = -\frac{\sigma_{ch}}{\varepsilon \varepsilon_0}, \; \frac{\partial c_i}{\partial r} = 0, \; u = v = 0 \tag{14d}$$

Boundary GH:

$$\phi_2 = 0, \psi = 0, \; c_i = c_0, \; p = 0 \tag{14e}$$

Boundary AH:

$$\frac{\partial \psi}{\partial r} = \frac{\partial \phi}{\partial r} = \frac{\partial c_i}{\partial r} = \frac{\partial u}{\partial r} = \frac{\partial v}{\partial r} = 0 \tag{14f}$$

5. NUMERICAL MODEL

Equations (7)-(12) along with the boundary conditions given in Eq. (14) were solved using the commercial code COMSOL 3.4 (http://www.comsol.com/). The finite element calculations were performed using quadratic triangular elements. Since the numerical solution accuracy depends strongly on the mesh size, a refined mesh is necessary in the region near the surface where the dependent variable gradients are pronounced. A finer mesh was used in this study near the charged surface to capture the subtle changes in the ion concentration and electrical potential. Solution independence in the mesh size was carefully studied before reporting the final results. Moreover, the current is computed using the weak constraints provided by the COMSOL. By solving the Lagrange multipliers along with the governing equations, accurate ionic flux can be obtained.

6. RESULTS AND DISCUSSION

KCl aqueous solutions at T=298K temperature were used as the working fluid. The dielectric constant of the KCl aqueous solution is 80, the molecular diffusivities of K^+ and Cl^- are 1.96×10^{-9} and 2.03×10^{-9} m^2/sec, respectively.

The density and viscosity of the solution are assumed to be 1000 kg/m^3 and 10^{-3} Pas, respectively. The bulk concentration c_0 is chosen in the range of 10^{-6} ~ 1 M. From the literature, nanochannel wall surface charge density depends on the channel material, pH value and ionic strength of bulk electrolyte [41, 42]. In this study, the charge density of the wall is chosen in the range of -5×10^{-3} to 5×10^{-3} C/m^2 in order to obtain reliable numerical solution. The nanochannel radius and length are varied in the ranges of 5 ~ 50 nm and 1 ~10 μm, respectively. The microchannel length L_1 is fixed at 1 μm while the radius (sidewall length) varies in the range of 0.5~1.5 μm.

For the chosen numerical parameters, we first examine the effect of EOF on the ionic transport through the nanochannel. Under the conditions of $\Delta\phi = 1$ V, $\sigma_{ch} = \sigma_w = -5\times10^{-3}$ C/m^2, L=5 μm, a=15 nm and $a_1 = 0.5$ μm, the computed nanochannel conductances with and without EOF as function of bulk concentration are compared and shown in Figure 4. The effect of EOF is visible but small. The ionic current is slightly increased because of the inclusion of convective current due to fluid flow [43, 44]. This result agrees with that reported in the study of Vlassiouk et al. [30]. As estimated by Daiguji et al. [23], the ratio of current due to EOF and current due to electromigration is around 7% for surface charge density with order of magnitude used in this study. Since we focus on the effect of entrance charge condition on the ionic transport through the nanochannel with low potential bias, the convective current is ignored for the results presented in the following. This assumption greatly simplified the computation because the Navier-Stokes equation was not solved. However, this assumption becomes

invalid as the applied voltage is higher than the voltage that resulting in limiting or over-limiting current. In such condition, the nonlinear I-V curve is resulted due to flow mixing by the vortical flow motion at the nanochannel entrance and exit [45-48].

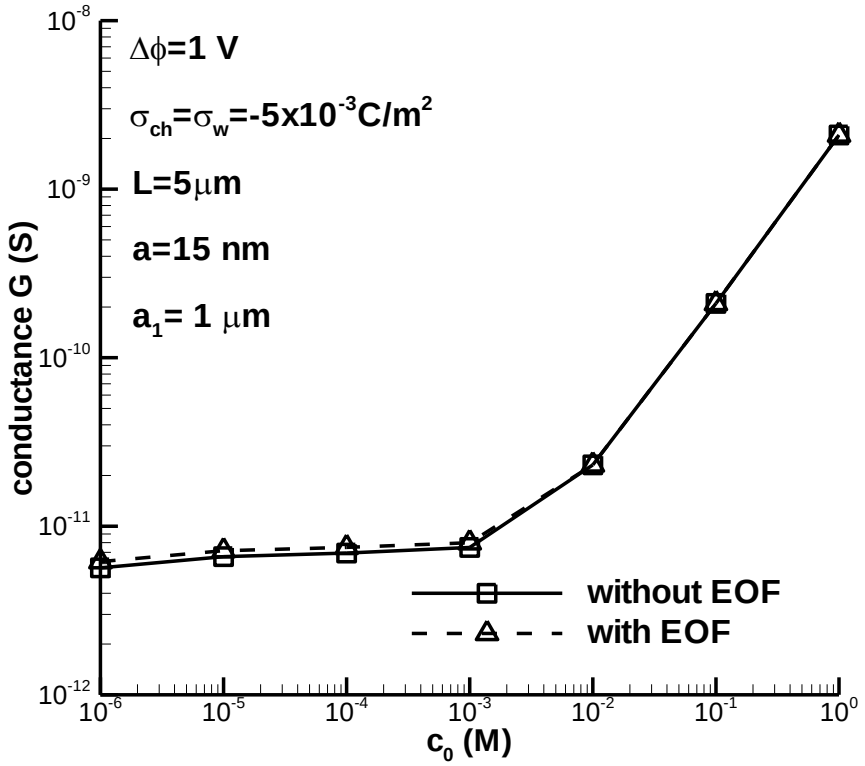

Figure 4. Effect of EOF on the nanochannel conductance as function of electrolyte bulk concentration.

(a)

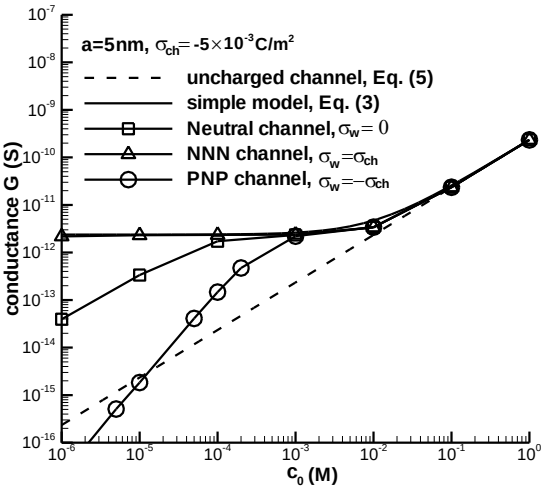

(b)

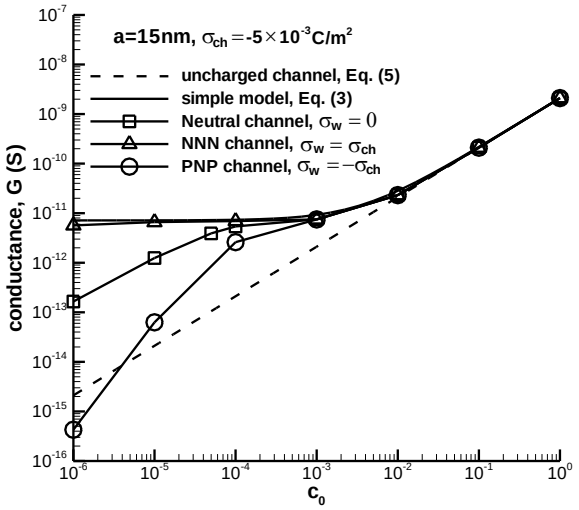

(c)

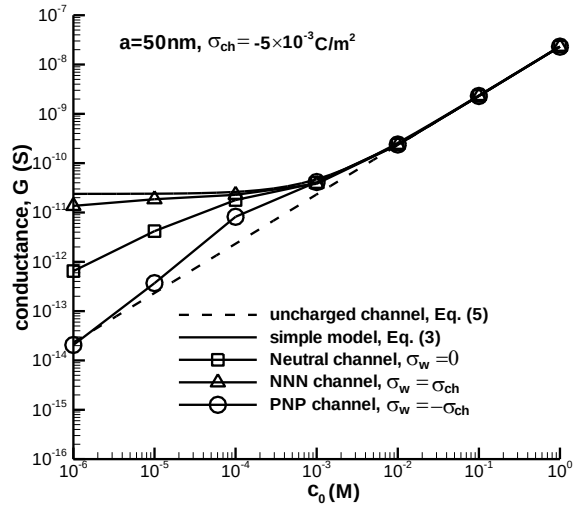

Figure 5. Nanochannel conductance as functions of nanochannel radius, electrolyte bulk concentration, and charged conditions in log-log scale plot. Model parameters are $\Delta\phi$=1 V, σ_{ch}=-5×10^{-3} C/m^2, L=5 μm, L$_1$=1 μm, and a_1=1 μm. The sidewall surface charge densities are σ_w=0, -5×10^{-3}, and 5×10^{-3} C/m^2 for Neutral, NNN, and PNP channels, respectively. (a) a=5 nm. (b) a=15 nm. (c) a=50 nm.

Using the same conditions for the Figure 4, the conductance of the Neutral, NNN, and PNP channels as function of electrolyte bulk concentration and nanochannel radius are shown in Figure 5. The results were compared with that predicted by the simple model and uncharged channels described in Eqs. (3) and (5), respectively. As shown in Figure 5, the predicted NNN channel conductance is in good agreement with Eq. (3) for all the channel sizes studied.

That is, the conductance plateau can be obtained in the low-salt regime in the log-log scale plots. However, a slight deviation was found in the low-salt regime. The reason for this deviation may be attributed to the exclusion of access resistance in the simple model. As the bulk concentration is

(a)

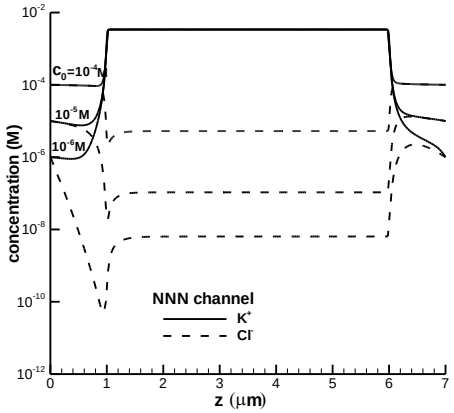

(b)

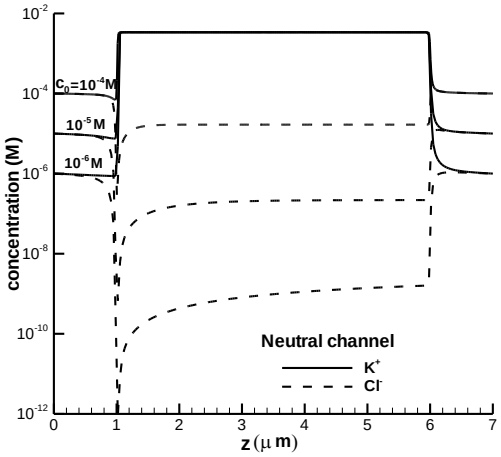

(c)

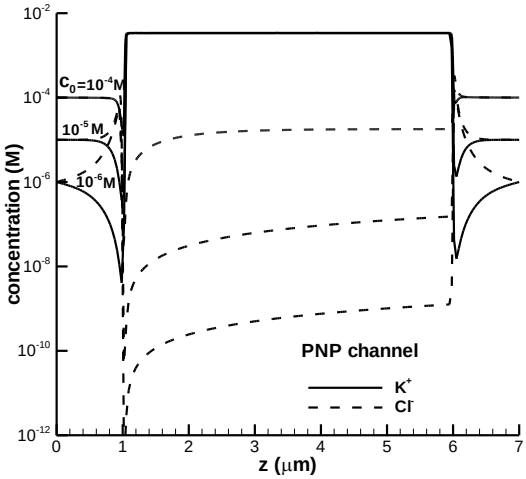

Figure 6. Ionic concentration distribution along the channel centerline for $c_0 = 10^{-6} \sim 10^{-4}$ M and a =15 nm. Model parameters are the same as those in Figure 4. (a) NNN channel, (b) Neutral channel, (c) PNP channel.

large, a linear relation between bulk concentration and nanochannel conductance resulted. The agreement between the results predicted by the simple model and numerical mode for the high-salt regime are also good. For both Neutral and PNP channels, the conductance plateau can only be found

(a)

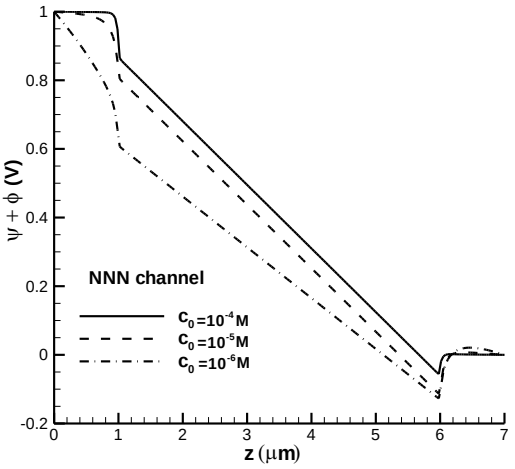

(b)

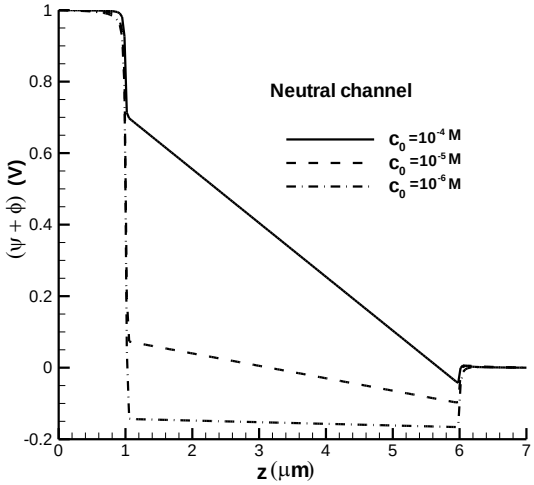

(c)

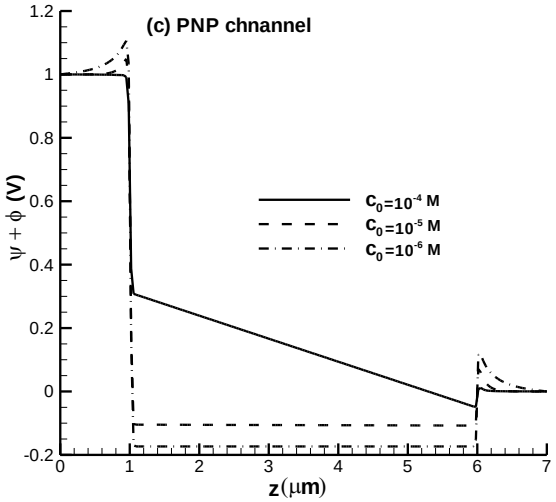

Figure 7. Potential distribution along the channel centerline for c_0 =10^{-6} ~10^{-4} M and a =15nm. Model parameters are the same as those in Figure 4. (a) NNN channel, (b) Neutral channel, (c) PNP channel.

when the bulk concentration is in the range around the transition bulk electrolyte c_t which is approximately equal to $0.5\,c_e$ [21].

For bulk concentration lower than c_t, a nearly linear relation between the bulk concentration and conductance was found for the Neutral and PNP channels. At very low bulk concentration and small nanochannel, the nanochannel channel conductance can be lower than the uncharged channel predicted by Eq. (5) for PNP channel.

To further understand the results obtained in Figure 5, we compare the ionic and potential distributions in the low-salt regime along the centerline of the nanochannel for the Neutral, NNN and PNP channels as shown in Figures 6 and 7, respectively. The numerical parameters used in Figures 6 and 7 are the same as those in Figure 5 except that we focus on the a =15 nm case. As shown in Figure 6, the concentration polarization occurs at the nanochannel entrance and exit as the externally potential bias is applied [4, 5, 33, 46] for the three types of channel studied. The counterion (K^+) concentrations inside the nanochannel for all three types of channels have the same magnitude because of the same nanochannel surface charge density. The co-ion concentration has a small value due to the electrostatic depletion. As shown in Figure 6, the co-ion concentration depends on the bulk concentration or the degree of electric double layer (EDL) overlap. More significant coion depletion by electrostatic effect is resulted when the EDL overlap is more serious [4, 23]. Based on the concentration distribution characteristics, the major current carrier is the counterion because the coion concentration is much smaller than the counterion. Therefore, it should be expected that the current for all channels should be approximately equal. However, Figure 6 shows that the concentration polarization at the nanochannel entrance and exit depends on both the bulk concentration and sidewall charge polarity. Correspondingly, the potential distribution along the channel is then also dependent on the bulk concentration and sidewall charge polarity, as shown in Figure 7. It is seen that the NNN channel has a smaller potential drop at the nanochannel entrance compared with Neutral and PNP channels because of enriched counterion due to negative charged sidewalls. Consequently, higher electric field and electric current can be obtained in the NNN channel. It is also interesting to point out that a very low electric field results when the bulk concentration is low. In the PNP channel, almost zero electric field is found when the electrolyte bulk concentration is low. Based on the results shown in Figures 6 and 7, it can be concluded that the degree of concentration polarization depends on the bulk concentration, applied potential bias, and sidewall charge condition. The concentration polarization induced potential drop at the nanochannel entrance controls the current flow through the nanochannel.

Based on the results shown in Figure 5, the experimentally observed conductance plateau in low-salt regime can only be obtained from the NNN channels having the same surface charge density magnitude and polarity, ie, the homogeneous charged channel. Using conductance of uncharged nanochannel G_0 described in Eq. (5) and Debye length defined as $\kappa^{-1} = (\frac{2Fc_0}{\varepsilon\varepsilon_0 RT})^{1/2}$ to normalize the nanochannel conductance and radius, respectively, the normalized nanochannel conductance as function of dimensionless nanochannel radius κa is shown in Figure 8. It is seen that the nanochannel conductance is enhanced in the low-salt regime. The conductance enhancement can be obtained as κa

is less than approximately 5 indicating that the conductance enhancement can be obtained even when the EDL is not overlapped. This result agrees with the experimental measurements of Liu et al. [22].

In Figure 9, the size effect on the homogeneous NNN channel conductance are shown using various sidewall lengths and nanochannel lengths under the fixed parameters of a=15 nm, $\Delta\phi$=1 V, and $\sigma_{ch} = \sigma_w$=- 5×10^{-3} C/m^2. For the chosen ranges of a_1 and L, the conductance plateau can be obtained as shown in Figure 8.

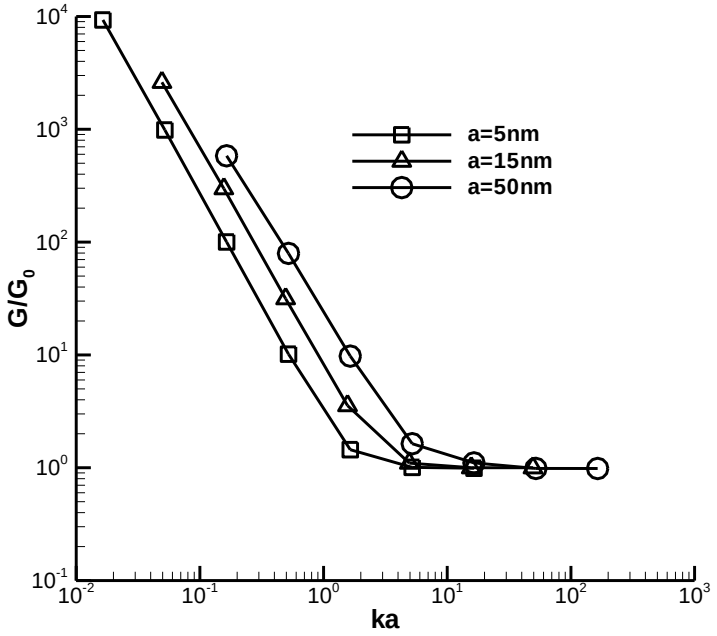

Figure 8. Normalized nanochannel conductance as function of dimensionless nanochannel radius κa. Model parameters are the same as those indicated in Figure 4.

(a)

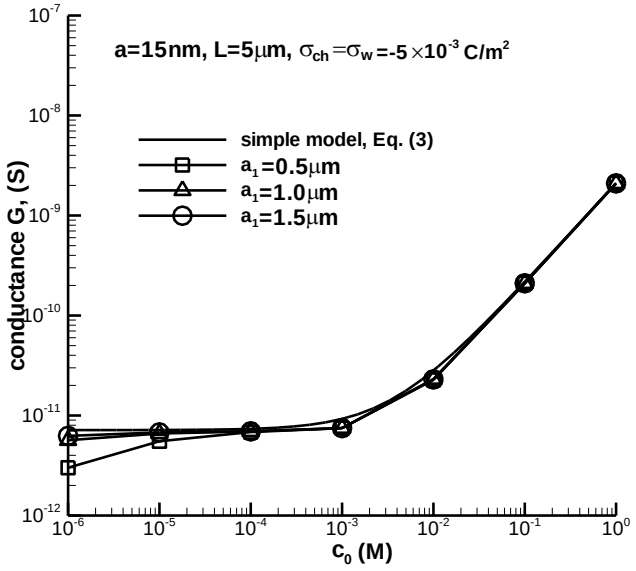

(b)

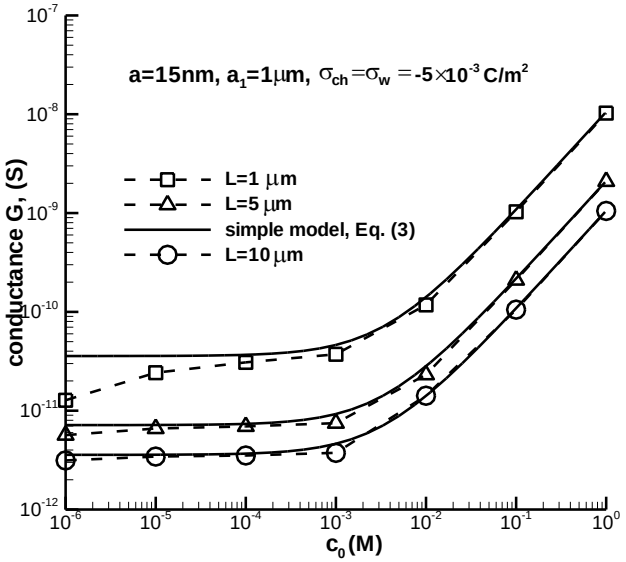

Figure 9. Size effect on the NNN channel conductance as function of electrolyte bulk concentration in log-log scale plot. (a) Effect of sidewall length. (b) Effect of nanochannel length.

For varied sidewall length cases shown in Figure 9(a), it is seen that the access resistance is reduced as the sidewall length increases. That is, more counterions can be attracted into the nanochannel entrance region and increases the current flow. The nanochannel length effect on the conductance shown in Figure 9(b) indicates that larger deviation between the simple model and numerically predicted conductance can be found for short nanochannel cases. The increase in electric resistance may be due to more serious concentration polarization due to high electric field when the nanochannel is short. It also implies that the simple nanochannel conductance model (Eq. (3)) is valid only for long channels [30].

(a)

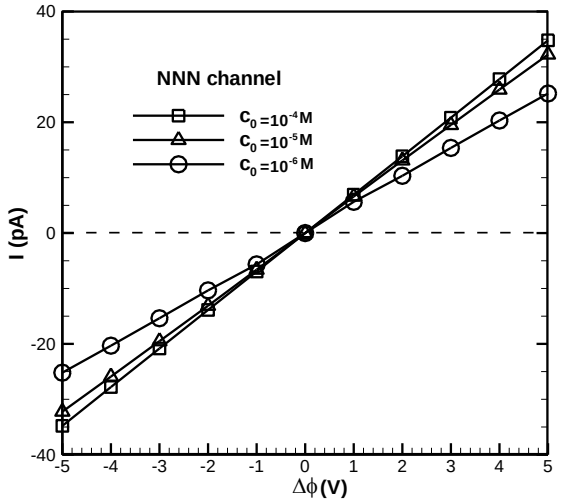

(b)

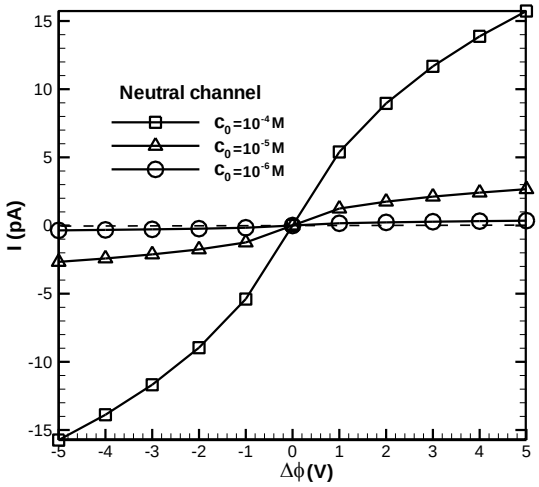

(c)

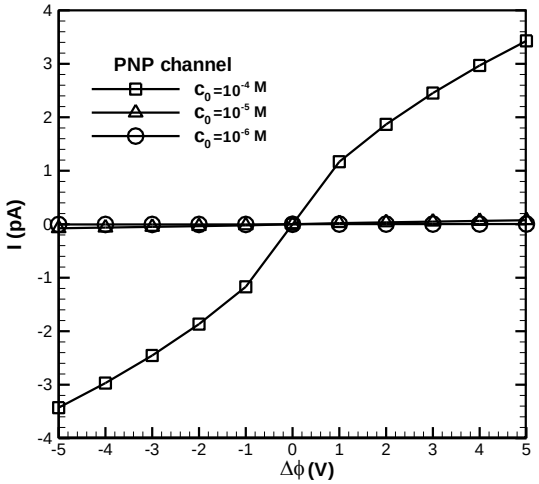

Figure 10. I-V curves of (a) NNN channel, (b) Neutral channel, and (c) PNP channels for $c_0 = 10^{-6} \sim 10^{-4}$ M and a =15nm. Model parameters are the same as those in Figure 4 except that the applied potential bias $\Delta\phi$ varies between -5 and 5 V.

Figure 10 depicts the I-V curve characteristics for the Neutral, NNN, and PNP channels. We examine the I-V curves for the low bulk concentration regimes because large variations are expected. For all the I-V curves shown in Figure 10, there is no current rectification because of the symmetric charge arrangement with respect to the nanochannel center [6]. For the NNN channel as shown in Figure 10(a), the I-V curve maintains linear relation in the low-salt regime. Because of the concentration polarization effect, deviations in current for the three bulk concentrations become more significant when the potential bias is large. For the Neutral channel shown in Figure 10(b), nonlinear I-V curve was found in the low-salt regimes. Without the counterion enrichment by the sidewall charge, the current magnitudes are small compared with the NNN channel, especially for the low bulk concentration cases (10^{-5} and 10^{-6} M).

(a)

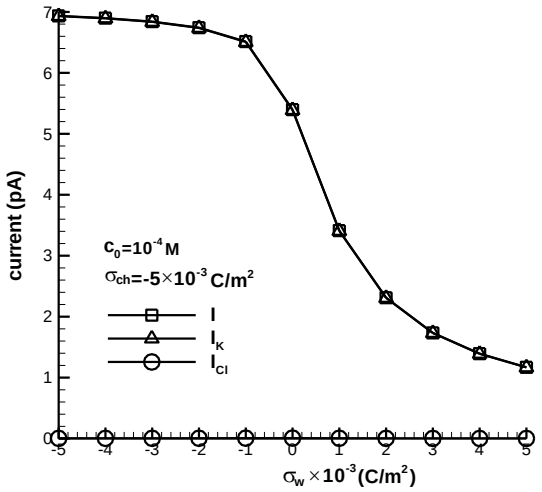

(b)

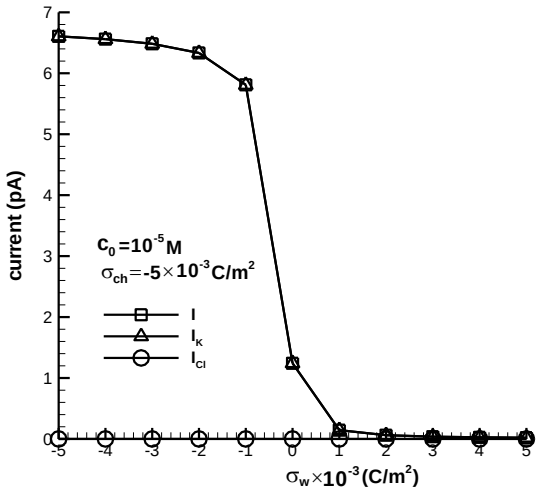

(c)

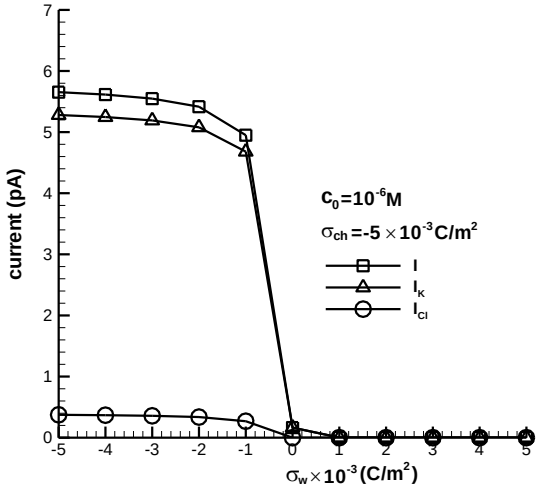

Figure 11. Current flow as a function of the sidewall charge density varied in the range of $-5\times10^{-3}\sim 5\times10^{-3}$ C/m^2. Model parameters are the same as those in Figure 4 except that the nanochannel radius is fixed as a=15 nm. (a) c_0=10^{-4} M, (b) c_0=10^{-5} M, and (c) c_0=10^{-6} M.

Because of counterion was expelled at the nanochannel entrance by the positively charged wall, the current flow in PNP channel shown in Figure 10(c) is much smaller than those in NNN and Neutral channels as the bulk concentration is low.

As mentioned earlier, the present study focuses on the ionic transport in the Ohmic regime with low applied voltage bias. For applied voltage used in Figure 10, there is no limiting or over-limiting occurs. This indicates that the I-V relation is in Ohmic regime [49]. As the applied voltage is high enough, nonlinear I-V curve is resulted. Under such circumstance, larger computational domain and EOF should be considered [45-48].

Finally we examine the effect of sidewall surface charge density magnitude on the current flow characteristics in the nanochannel, as shown in Figure 11. In Figure 11, I_{K^+}, I_{Cl^-}, and I are the current carried by K^+, current carried by Cl^-, and the total current ($I_{K^+} + I_{Cl^-}$), respectively. The nanochannel surface charge density and applied potential bias are fixed as $\sigma_{ch} = -5\times10^{-3}$ C/m^2 and $\Delta\phi$=1 V, respectively. For all the bulk concentrations studied, Figure 11 shows that the major current carrier is K^+ while the current carried by Cl^- is relatively small. For the c_0 =10^{-4} M case shown in Figure 11(a), the current decreases slightly with the decrease in absolute surface charge density magnitude when the sidewall is negatively charged, which has the same polarity as the nanochannel. When sidewall is positively charged the current flow in the nanochannel decreases as the surface charge density increases. For the low bulk concentration cases shown in Figures 11(b) and 11(c), the current also decreases with the decrease in absolute charge density magnitude when the sidewall is negatively charged. When the sidewall is positively charged, which is opposite to that of the nanochannel, the current decreases drastically. Based on the results shown in Figures 11(b) and 11(c), it implies that it is possible to switch on or off the current using the sidewall charge polarity. That is, a nanofluidic switch can be constructed. For the negatively charged nanochannel, the negatively charged sidewall corresponds to the ON mode of the nanofluidic switch while the OFF mode corresponds to the positively charged sidewalls.

The results shown in Figure 11 have clearly indicated the nanofluidic switch can be constructed by controlling the sidewall charge condition when bulk concentration is low (10^{-5} and 10^{-6}M). For high bulk concentration case (10^{-4}M), the nanofluidic switch is not sensitive by controlling the sidewall charge condition. Based on this result, we may conclude that one of the factors affecting the nanofluidic switch sensitivity would be the degree of electric double layer (EDL) overlap, ie, the value of dimensionless nanochannel radius ka. When ka is large, nanofluidic switch using the proposed method is not sensitive. Besides ka, the sensitivity of nanofluidic switch may also depend on several parameters such as sidewall surface charge density and length, applied electric field strength, microchannel length, and nanochannel size and surface charge density. To be consistent with the primary goal of the present study, effects of charged sidewall length, nanochannel surface charge density, and nanochannel radius on the nanofluidic switch sensitivity are performed for more detail understanding of the capability of the proposed method. The increase of charged sidewall length has the effect of attracting or depleting more counterions in the nanochannel entrance region, depending on the sidewall charge polarity. By changing the nanochannel size, the effect of EDL overlap on current switching can be examined.

(a)

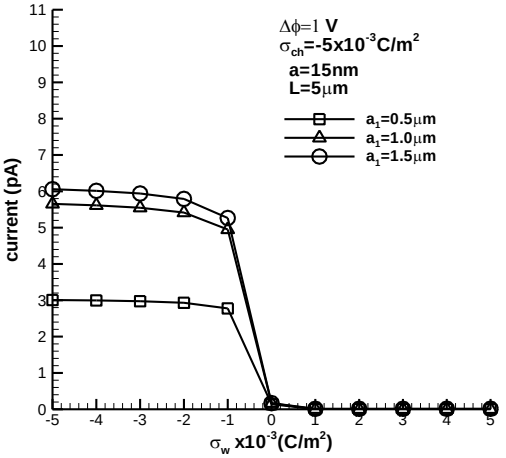

(b)

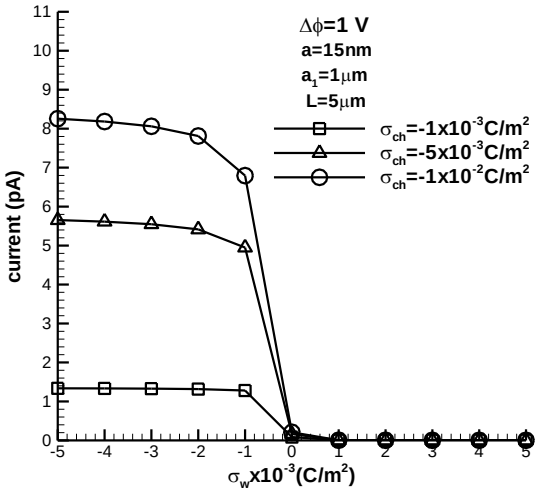

(c)

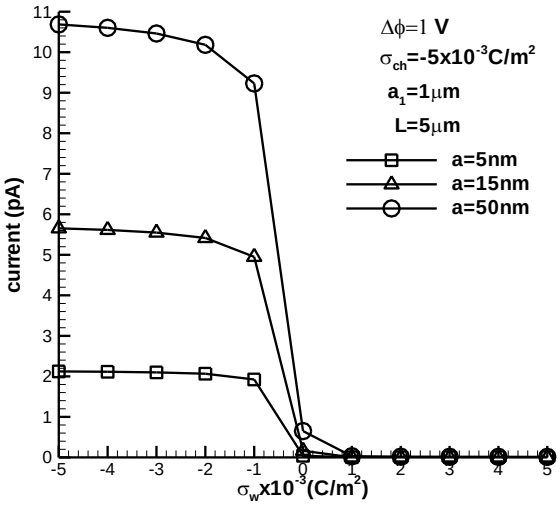

Figure 12. Nanofluidic switch characteristics with $c_0 = 10^{-6}$ M. (a) Effect of charged sidewall length, (b) Effect of nanochannel surface charge density. (c) Effect of nanochannel size.

The increase of nanochannel surface charge density can enhance the counterion concentration inside the nanochannel and can be used to examine the capability of sidewall charge density magnitude on current switching. In order to keep the micro-nanochannel system under the same externally applied electric field, the uncharged microchannel lengths are kept the same. As shown in Figure 12, the current switching by controlling the entrance charge condition can still be obtained by varying these parameters. This indicates that proposed method can be used to construct nanofluidic switch without using high sidewall surface charge densities.

7. CONCLUSIONS

This study examined the sidewall charge effect on the ionic transport characteristics in micro-nanochannel systems. Based on the results obtained in this study, the following conclusions can be made:

(1) To obtain the experimentally observed nanochannel conductance plateau with respect to the bulk concentration in log-log scale plot, the sidewall charge density must be the same as that of the nanochannel in both magnitude and polarity. That is, the wall charge must be homogeneous.

(2) For neutral (uncharged) sidewalls, the conductance plateau can only be found with bulk concentration near the transition bulk concentration. In the low bulk concentration regime, nanochannel conductance varies approximately linearly with the bulk concentration.

(3) For the sidewall charge having different polarity from the nanochannel, the nanochannel entrance and exit act like an electronic diode. The depletion of counterion near the nanochannel entrance produces less current flow through the nanochannel.

(4) It is possible to construct a nanofluidic switch by controlling the sidewall charge polarity. When the sidewall is charged with the same polarity as the nanochannel, it corresponds to the ON mode of the switch, while the OFF mode is operated by having the sidewall charged with polarity opposite that of the nanochannel. The sensitivity of current switch depends on the dimensionless nanochannel radius. For the proposed physical domain and chosen parameter ranges such as nanochannel size and surface charge density, and charged sidewall length, the numerical results indicated that the nanofluidic switch can be constructed without using high sidewall surface charged densities.

References

1. P. Abgrall, N.T. Nguyen *Anal. Chem*. 80(7) (2008) 2326
2. R.B. Schoch, J.Y. Han, P.Renaud, *Rev. Mod. Phys*. 80(3) (2008) 839
3. B. Zaltzman, I.J. Rubinstein, *J. Fluid Mech*. 579 (2007) 173
4. Q. Pu, J. Yun, H. Temkin, S. Liu, *Nano Lett*. 4 (2004) 1099
5. K. Zhou, M.L. Kovarik, S.C. Jacobson,. *J. Am. Chem. Soc.* 130 (2008) 8614
6. Z. Siwy, I.D. Kosinska, A Fulinski, C.R. Martin, *Phys. Rev. Lett*. 94 (2005) 048102
7. A. Holtzel, U. Tallarek, *J. Sep. Sci*. 30 (2007) 1398
8. Y.C. Wang, J. Han, *Lab Chip* 8 (2008) 392

9. J.H. Lee, Y.A. Song, S.R. Tannenbaum, J. Han, *J. Anal. Chem*. 80 (2008)3198
10. H.C. Chang, G. Yossifon,E.A. Demekhin, *Annu. Rev. Fluid Mech*. 44 (2012) 401
11. K. Schmidt-Rohr, Q. Chen, *Nat. Mater*. 7(1) (2008) 75
12. D. Hlushkou, R. Dhopeshwarkar, R.M. Crooks, U. Tallarek, *Lab Chip* 8(7) (2008) 1153
13. H. Daiguji, Y. Oka, K. Shirono, *Nano Lett* 5 (11) (2005) 2274
14. H. Daiguji, T. Adachi, N. Tatsumi, *Physical Review* E 78 (2008) 026301
15. I. Vlassiouk, Z. Siwy, *Nano Lett*. 7(3) (2007) 552
16. I. Vlassiouk, S. Smirnov, Z. Siwy, *ACS Nano* 2(8) (2008) 1589
17. D.K. Kim, C. Duan, Y.F. Chen, A. Majumdar, *Microfluid Nanofluid*. 9 (2010) 1215
18. C.C. Striemer, T.R. Gaborski, J.L. McGrath, P.M. Fauchet, *Nature* 445(7129) (2007) 749
19. D. Stein, M. Kruithof, C. Dekker, *Physical Review Letters* 93 (2004) 035901.
20. R. Karnik, R. Fan, M. Y., D. Li, P. Yang, A. Majumdar, *Nano lett*. 5(5) (2005) 943
21. R.B. Schoch, P. Renaud, *Applied Physics Letters* 86 (2005) 253111
22. S.R. Liu, Q.S. Pu, L. Gao, C. Korzeniewski, C. Matzke, *Nano Letters* 5 (2005) 1389
23. H. Daiguji, P.D. Yang, A. Majumdar, *Nano Letters* 4 (2004) 137
24. M. Wang, Q. Kang, E. Ben-Naim, *Analytica Chimica Acta* 664 (2010) 158
25. F.H.J. van der Heyden, D.J. Bonthuis, D. Stein, C. Meyer, C. Dekker, *Nano Letters* 7 (2007) 1022
26. Y.S. Choi, S.J. Kim, *J. Colloid Interface Sci*. 333 (2009) 672.
27. K. D. Huang, R. J. Yang, *Nanotechnology* 18(11) (2007) 115701
28. R. J. Hunter, Zeta Potential in Colloid Science: Principles and Applications, *Academic Press*, New York (1981)
29. M. Lobbus, J. Sonnfeld, H.P. van Leeuwen, W. Vogelsberger, J. Lyklema, *J. Colloid Interface Sci*. 229 (2000) 174
30. I. Vlassiouk, S. Smirnov, Z. Siwy, *Nano Lett*. 8(7) (2008) 1978
31. L.J Cheng, J. Guo, *Microfluidics and Nanofluidics.* 9(6) (2010)1033
32. T. Postler, Z. Slouka, M. Svoboda, M. Pribyl, D. Snita, *J. Colloid and Interface Sci.* 320 (1) (2008) 321
33. H.C. Chang, G. Yossifon, *Biomicrofluidics* 3 (2009) 012001
34. Z.S. Siwy, S. Howorka, *Chem. Soc. Rev*. 39 (2010) 1115
35. L.J. Cheng, J. Guo, *Chem. Soc. Rev*. 39 (2010) 923
36. M. Aguilella-Arzo, V. M. Aguilella, R. S. Eisenberg, *Eur. Biophys. J.* 34 (2005) 314
37. R.J. White, B. Zhang, S. Daniel, J.M. Tang, E.N. Ervin, P.S. Cremer, H.S. White, *Langmuir* 22 (2006) 10777
38. S. Qian, A. Wang, J.K. Afonien, *J. Colloid Interface Sci*. 303 (2006) 579.
39. H. Liu, S. Qian, H.H. Bau, Biophys. J. 92 (2007) 1164.
40. R.F Probstein, Physicochemical Hydrodynamics: An Introduction, 2nd ed., Wiely, New York (1994)
41. S.H. Behrens, D.G. Grier, *J. Chem. Phys*.115 (2001) 6716
42. J. Cervera, B. Schiedt, P. Ramırez, P. *Europhys. Lett.* 71 (2005) 35
43. X. Wang, J. Xue, L. Wang, W. Guo, W. Zhang1, Y. Wang, Q. Liu, H. Ji, Q. Ouyang, J. Phys. *D: Appl. Phys.* 40 (2007) 7077
44. H.S. White, A. Bund, *Langmuir* 24 (2008) 2212
45. G. Yossifon and H.C. Chang, *Phys. Rev. Lett*. 101 (2008) 254501
46. S. J. Kim, Y. C. Wang, J. H. Lee, H. Jang, and J. Han, *Phys. Rev. Lett*. 99 (2007) 044501
47. B. Zaltzman and I. Rubinstein, *J. Fluid Mech*. 579 (2007) 173
48. I. Rubinstein, B. Zaltzman, J. Pretz, and C. Linder, *Russ. J. Electrochem*. 38 (2000) 853
49. V.G. Levich, Physicochemical Hydrodynamics, Prentice-Hall, New York (1962)